

## **MnBi MAGNETIC MATERIAL: A CRITICAL REVIEW**

NGUYEN VAN VUONG,<sup>†</sup>

*Institute of Materials Science, Vietnam Academy of Science and Technology  
18, Hoang Quoc Viet, Cau Giay, Hanoi, Vietnam*

<sup>†</sup>*E-mail:* vuongnv@ims.vast.ac.vn

*Received 21 August 2019*

*Accepted for publication 12 September 2019*

*Published 25 October 2019*

**Abstract.** *Manganese Bismuth (MnBi) - the ferromagnetic material attracting a great interest of the world magnetic society last years. The absence of rare-earth elements in compositions, the large magnetocrystalline anisotropy, the room-temperature moderate but high-temperature reasonable magnetization plus the positive temperature coefficient of coercivity and the moderate Curie temperature make MnBi bulk magnets very potential for high-temperature magnet application. This bright future is a little gray because the research results in the past were not as expected. The paper summarizes the results concerning the MnBi alloys, powders and bulk magnets investigated during past 67 years. The look on the difficulties inhibiting the development of this material is given and the proposals that might allow overcoming the difficulties and push again the efforts of research towards the goal of 12 MGOe for the energy product  $(BH)_{max}$  of MnBi bulk magnets are discussed.*

**Keywords:** MnBi; low-temperature phase; magnetization; coercivity; energy product; bulk magnets.

**Classification numbers:** 61.05.cp; 75.30.Gw; 75.50.Ww; 75.60.Ej.

## I. INTRODUCTION

The rare-earth-free low-cost MnBi magnets with the energy product  $(BH)_{max}$  competitive with NdFeB bonded magnets in room-temperature (RT) as well with NdFeB sintered magnets in high-temperature (150 – 200°C) applications attract great attentions of scientific community. However, despite the spent efforts, the current best  $(BH)_{max}$  value of MnBi bulk magnets is only 8.4 MGOe [1], a half of the theoretical limit of 18.5 MGOe.

This paper presents a short survey concerning the status of MnBi hard magnetic material and bulk magnets prepared thereof. The reasons, including the principle and technical ones restricting the performance of magnets are discussed in detail. The actual results concerning the efforts of finding novel techniques to overcome the restrictions are also discussed.

The review consists of four parts. Beside the introduction part I, part II gives a brief look of the magnetism of MnBi system, concerning its crystal structure, magnetic configuration, its magnetization and coercivity as well their temperature dependences. Part III presents the status of preparation of MnBi bulk magnets. The used methods of preparation, the magnetic properties of obtained bulk magnets are summarized and the way to get high-performance MnBi bulk magnets is discussed. Part IV lists the conclusions on the future development of the MnBi materials and bulk magnets prepared thereof. A unique problem which must be solved in order to have a bright future of this rare-earth-free MnBi magnets is highlighted.

## II. MAGNETISM OF MnBi MATERIAL

### II.1. Magnetization

The MnBi hard magnetic material is prepared by alloying Mn and Bi substances. In the periodic table, although Mn is located just before the ferromagnetic elements Fe, Co and Ni, but is antiferromagnetic at RT. The substance Bi is known as non-magnetic material.

The combination of these two substances changes exchange coupling existed in the unit cell of MnBi materials, which can lead to ferromagnetism depending on the coupling intensity. Ordinary, the coupling strength depends on the ratio  $\lambda$  between the interatomic distance and radius of d-shell of Mn atoms in the unit cell, this dependence is described by the known Bethe-Slater curve [2]. In the case of pure Mn, the  $\lambda$  value is just below 1.5, which is slightly less than that of its ferromagnetic neighbors Fe, Co and Ni. This implies that increasing the separation between Mn atoms will favorably alter the ratio  $\lambda$  and leading to ferromagnetism. In particular, this evidence is realized by alloying Mn with Bi and the MnBi alloys become ferromagnetic. As discussed in [3], the value of the critical Mn - Mn distance for the onset of ferromagnetism in NiAs type compounds is equal to the critical distance derived by Forrer after examining a large number of materials which own their ferromagnetism predominantly to the direct exchange interaction. For Mn ions this distance equals 2.83 Å.

The ferromagnetic phase (from here and after this phase is named as LTP – Low Temperature Phase since it is formed only below 613 K) of MnBi is crystallized in the NiAs-type structure [4] (see Fig. 1). The unit cell of LTP MnBi belongs to the hexagonal system with six- and three-fold symmetry, is primitive with two mirror and one glide planes, so the space group is  $P6_3/mmc$ . The standard powdered X-ray diffraction (XRD) pattern is PDF#03-065-8164, the unit cell parameters are  $4.28 \cdot 4.28 \cdot 6.11$  Å,  $\langle 90.0 \cdot 90.0 \cdot 120.0^\circ \rangle$ , the Rontghen mass density  $\rho = 9.042$  g/cm<sup>3</sup> and the unit cell volume is 96.93 Å<sup>3</sup>. By using the X-ray radiation with  $K_\alpha$  line

of wavelength 1.5406 Å, the strongest peak (101) of LTP MnBi is located at the scattering angle  $2\theta = 28.14^\circ$ .

The  $M_s$  of MnBi compound comes from the magnetic moments of Mn atoms located in the unit cell and affected by the all terms of exchange interactions  $J_i$  figured in this cell built. The complicated scenario of exchange interactions is considered in [5] with six terms of  $J_i$  schematically marked in Fig. 1. In [5], the inelastic neutron scattering to investigate the magnetic structure of MnBi through the spin wave measurements was applied. The results revealed that, the nearest-neighbor term is antiferromagnetic, and the realization of a ferromagnetic ground state relies on the more numerous ferromagnetic terms beyond nearest neighbor, suggesting that the ferromagnetic ground state arises as a consequence of the long-ranged interactions in the system.

The experimental value of  $M_s$  was reported in [1]. To evaluate  $M_s$  of LTP MnBi compound, the pure Mn and Bi were weighted in the atomic percent ratio 1 : 1 and arc-melted thrice. The arc-melted alloy was, by hand, ground into powder and annealed at 563 K for 24 h. The final powder was further ball-milled to reduce the particle size  $\sim 5 \mu\text{m}$ , aligned in an 18 kG magnetic field and hot-compacted at 530 K for 30 min. to achieve the magnet density  $\rho_m \approx 8.4 \text{ g/cm}^3$ . The sample LTP content was determined by Rietveld refinement of the neutron diffraction pattern of ground powders and equals 91.1 wt%.  $M_s$  of LTP MnBi material was determined by using the saturation magnetization of aligned magnet measured at 90 kOe field oriented parallel to the alignment direction. By this strong field, the measured saturation magnetization can be considered as the spontaneous magnetization  $M_s$ . According to [1], the RT measured magnetization is 74 emu/g, corresponding to the RT  $M_s = 81.3 \text{ emu/g}$  and thus  $3.84 \mu\text{B}$  per Mn atom at this temperature for MnBi material with 100 wt% of LTP content.

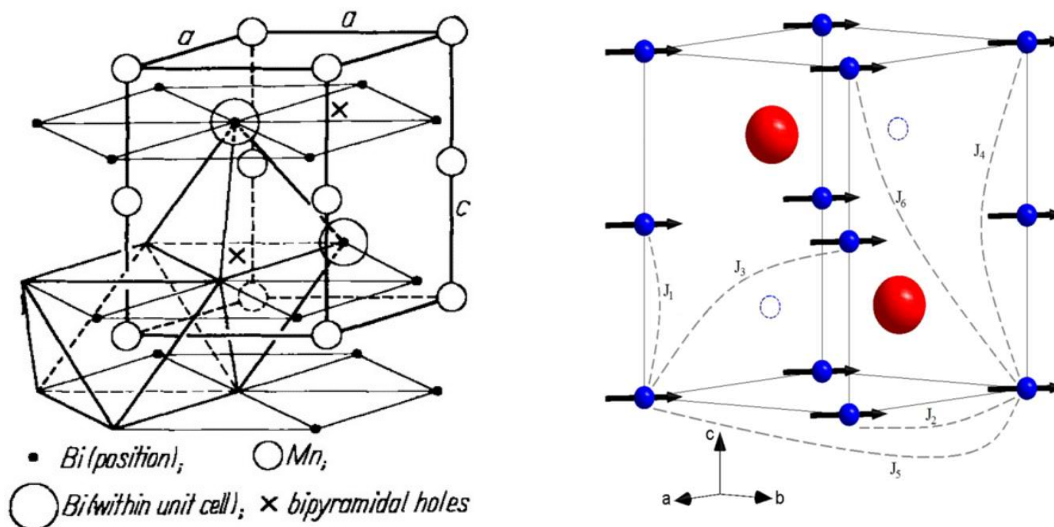


**Fig. 1.** Unit cell of LTP MnBi crystal (left picture) [4] and six terms of exchange interaction  $J_i$  figured in this unit cell to establish the unit cell magnetic moment (right) [5].

This value of  $M_s$  was supported by the  $M(H)$  curve measured at RT for a perfect melt-spun ribbon sample presented in Fig. 2. The ribbon sample was prepared by rejecting the melt of highly

LTP-content MnBi alloy on the cooper wheel rotated with the tangent speed 18 m/s. It is worthy to note that, in the case study, the wheel was equipped with the permanent magnet system creating the surface magnetic field of 3 kOe perpendicular to the wheel surface. The magnetic field assisted melt-spinning technique enhanced the formation of LTP MnBi ribbon as did for Nd-Fe-B one [6].

The temperature dependences of crystal structure and related magnetic structure was investigated in [7]. The samples were melt-spun ribbons with RT LTP content of around 95 wt%. One observes that, the parameter of basal plane  $a=b$  is weakly temperature dependent, meanwhile the parameter  $c$  is obviously changed with temperature. The Rietveld refinement revealed that Mn-Mn distance is increased monotonically from 10 to 600 K. The magnetic moments of Mn atoms turn to align along the  $c$ -axis around 90 K, which is attributed to the spin reorientation at this temperature. So, the combination of these features leads to the moderate temperature dependence  $M_s(T)$  for LTP MnBi material measured in [1]. The similar behavior of  $M_s(T)$  observed in [8, 9] is plotted in the inset of Fig. 3. The theoretical curve is smooth and goes to zero at 711 K, however the experimental curve has an abrupt drop of magnetization at 633 K corresponding to the real value of  $T_c = 633$  K [10]. Before the abrupt drop at  $T_c$ ,  $M_s$  decreases linearly with the coefficient  $\beta = -(0.06 \div 0.07)$  emu/gK.

## II.2. Coercivity

As any hard magnetic materials, MnBi is available to work in an external magnetic field without losing its magnetization. The coercivity depends on spin – orbital interactions and is expressed through the magnetocrystalline anisotropy energy density  $E_u$  (the energy per volume unit). For MnBi belonging to the hexagonal crystal structure, in the second approximation  $E_u = K_1 \cos^2 \theta + K_2 \cos^4 \theta$  with  $\theta$  an angle between the easy axis and the external magnetic field. Roughly  $E_u$  is understood as the energy consumed for rotating the magnetic moment being parallel to the easy axis to the basal plane. The magnetocrystalline energy coefficients are  $K_1 =$

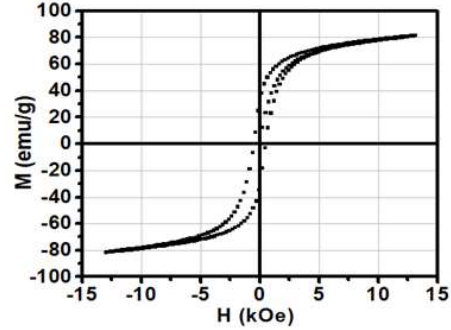


**Fig. 2.**  $M(H)$  loop of a perfect LTP MnBi ribbon sample with  $M = 81$  emu/g at 13.5 kOe.

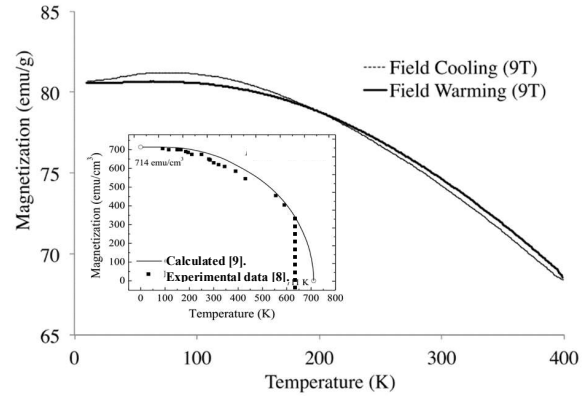


**Fig. 3.**  $M_s(T)$  of LTP powder measured at 90 kG [1]. The inset shows experimental [8] and calculated data [9] of  $M_s(T)$ . The dashed line is the  $M_s$  abrupt at  $T_c = 633$  K [19].

0.89 MJ/m<sup>3</sup> and  $K_2 = 0.27 \text{ MJ/m}^3$  [11], so MnBi owns the uniaxial easy axis along the c-axis of unit cell since these coefficients satisfy the condition:  $K_1 > 0$  and  $K_2 > -K_1$ .

The magnetocrystalline anisotropy energy determines the upper limit of coercivity  $iH_c$  of the pure LTP MnBi compound. This limit equals the ideal nucleation field  $H_N$  associated with two intrinsic parameters of material  $K_u$  and  $M_s$ ,  $H_N = 2K_u/M_s$  [12]. For MnBi, by using the approximation  $K_u \approx K_1 + 2K_2$  [8],  $M_s = 81.3 \text{ emu/g}$  and  $\rho = 9.042 \text{ g/cm}^3$ , this limit, at room temperature is estimated approximately  $H_N = 39 \text{ kOe}$ . Depending on the methods of estimation of  $K_u$ ,  $H_N$  suffers a great fluctuation, up to 56 kOe as announced in [13]. Particularly, this upper limit of coercivity should be for a dense MnBi bulk magnet owning an ideal microstructure with non-defected, non-interacted, single-domain-sized, and perfectly aligned grains assembly. Any deviation from these evidences leads to the reduction of  $iH_c$  far from this theoretical limit. So, the high value of  $iH_c \approx 30 \text{ kOe}$  was observed for monocrystalline samples grown from the eutectic melt of Bi-rich compositions [14]. The ratio between  $iH_c$  of real magnets to  $H_N$  of materials used for making magnets is around 50 – 60% as calculated in [15]. There is the linear dependence between  $H_N$  and  $iH_c$  for MnBi alloys in the wide range of temperature as reported in Ref. [16]. Unlike  $M_s$ , although being associated with  $E_u$  which, in turn, depends on the electronic structure of materials, the coercivity is not pure intrinsic property of magnets. A drop of coercivity from the upper limit of  $H_N$  depends on the perfection of powders used for making magnets and on the route of producing magnets.

Since, the MnBi bulk magnets are prepared using the powder metallurgy method, so the grinding process of MnBi alloys is compulsory. The nature of  $iH_c$  versus grain sizes  $D$  dependence is the change of domain microstructure from a normally distributed assembly of multi-domains grains of as-cast and as-annealed MnBi alloys (see region IV, Fig. 4 [13]) to the multi-domain but ordered assembly of micrometer-sized grains of ground MnBi powders, where the curling and buckling modes of magnetization reversal can happen (region III). By further reduction of  $D$ ,  $iH_c$  stays on a plateau of maximum for the assembly of ordered single-domain-sized ( $\sim 0.25 \mu\text{m}$ ) non-interacted grains (region II) followed by an abrupt drop (region I) for very fine ( $\ll 0.25 \mu\text{m}$ ) grains assembly. This region appears because the averaged (over small grain volumes) magnetocrystalline anisotropy energy is significantly decreased leading to the superparamagnetism.

The dependence  $iH_c(D)$  was studied experimentally in [17–20], the results affirmed the above said tendency. By increasing the ball-milling times  $t_m$ , the  $iH_c$  of milled powders first increases, reaching a plateau and slightly drops when the grain size becomes smaller the domain size of  $\sim 0.25 \mu\text{m}$  (see the inset of Fig. 5). The direct dependence between  $iH_c$  and the grain sizes  $D$  was reported in [19] and is reloaded in Fig. 5

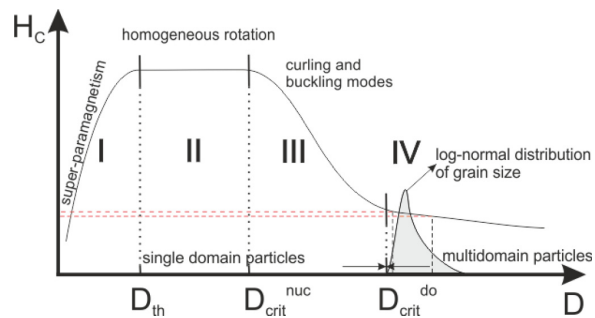


**Fig. 4.** The scheme of variation of coercivity  $H_c$  versus reduction of grain size  $D$  for ferromagnetic solids [13].

It is very important to note that, the  $iH_c(D)$  dependence of non-compacted powders is far from the  $iH_c(D)$  of compacted, aligned grains and sintered bulk magnets. Depending on the alignment technique, on the compaction and the sintering conditions, the coercivity  $iH_c$  of bulk sintered magnets is less than that of the green powders. This loss of  $iH_c$  is caused by the energy minimizing of the system of compacted and sintered magnets. This effect leads to the complicated process for optimizing the relationship between the grain size distribution of green powders, the pressure of compaction and the mass density  $\rho$  of final sintered bulk magnets. The very dense magnet with over-larged value of  $\rho$  increases the density of magnetic moment in the given volume of magnets but decreases the coercivity and hence the squareness of magnets. The porous magnet with low  $\rho$  serves a high  $iH_c$  but low remanence  $M_r$ . These evidences create an unbalance between  $M_r$  and remanence coercivity  $bH_c$  thus leads to the reduction of magnet energy product  $(BH)_{max}$ .

Within the fixed grain size distribution, the grain microstructure features such as phase distribution, morphology, and defects affect significantly on the coercivity mechanism and the coercivity values of magnets. The phase composition and distribution are crucial problems in establishing coercivity of MnBi bulk magnets. The multi-phase morphology of MnBi alloys as well the ground powders is closely connected with the peritectic nature of solidification of Mn-Bi system, which is clarified on the system phase diagram shown in Fig. 6.

The LTP MnBi is solidified from the melt of  $Mn_{50}Bi_{50}$  along the vertical arrow. Depending on the cooling rate, the MnBi alloy is solidified with the inclusions of Mn and Bi, the concentrations of which are varied by the ratio between the arms oa and ob, respectively. Besides, the ferromagnetic phase MnBi LTP forms only when the temperature is below 613 K, otherwise the phase should be paramagnetic with the composition  $Mn_{1.08}Bi$ . The compositions left from the point c (see Fig. 6) solidify Mn-Bi alloys containing only LTP and Bi, so the eutectic composition at the point d was used for crystalizing monocrystalline sample of LTP in the melt of Bi.

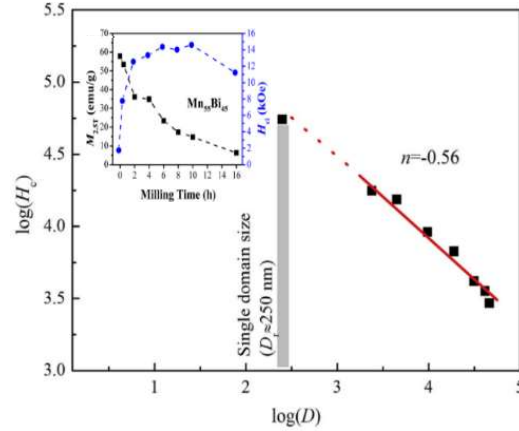


**Fig. 5.** The  $iH_c$  (in kOe) vs  $D$  (in nm) adopted from [19] and ball-milling times (see the inset [20]).

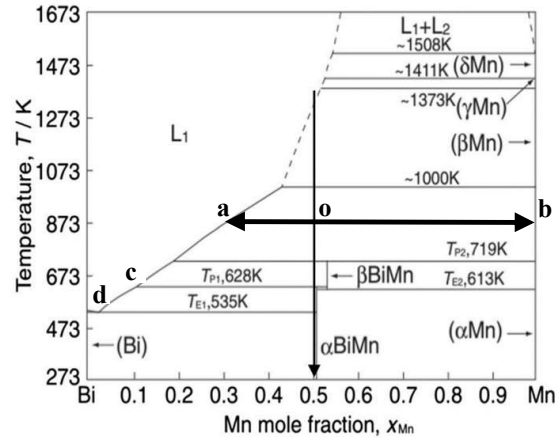


**Fig. 6.** The binary phase diagram of Mn-Bi system adopted from Ref. [21].

The mentioned feature of the phase diagram prevents alloying the pure LTP composition. The MnBi alloys contain LTP regions surrounded by Bi and Mn inclusions as observed in all samples prepared by different methods and by different investigators working in different laboratories. A typical picture of this multi-phase microstructure of arc-melted alloy samples can be seen on the SEM-micrographs taken by the table scanning electron microscope TM3000 of Fig. 7 adopted from Ref. [22]. The authors of this work demonstrates that different cooling rates regulated by the self-mass of batches (1g, 3g and 8g for a, b and c pictures, respectively) create different sizes of MnBi (grey color), Bi (white) and Mn (black) phase regions. The lower cooling rate the bigger region sizes.

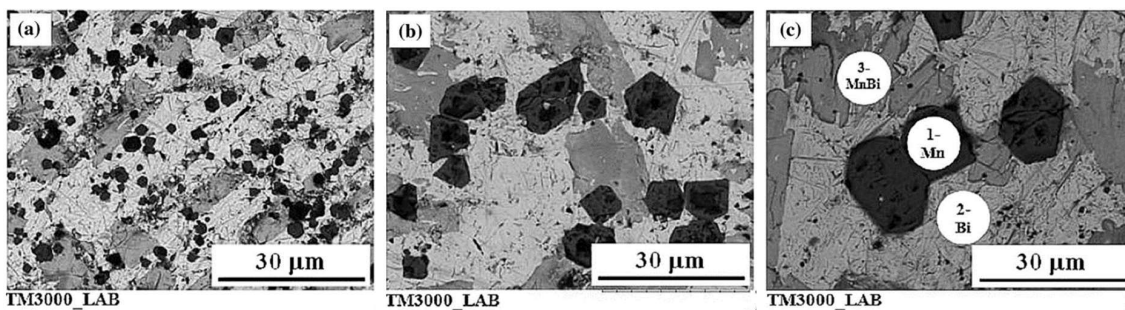


**Fig. 7.** The SEM-microstructures of as-cast arc-melted MnBi alloys. The pictures are adopted from Ref. [22].

Since in as-cast arc-melted alloys the LTP content is low, less than 30 wt%, to increase the magnetization the annealing process is completely required. Parallel to the mentioned multi-phase feature, there is the effect of separation and accumulation of low melting Bi (at 544 K) into clusters. These clusters, one side, hamper the LTP content enhancement to keep  $M_s$  on the low level and other side, reduce the isolation layers between LTP regions and thus effect on the coercivity.

In principle, the mixed microstructure of non-magnetic Bi and antiferromagnetic Mn inclusions should enhance the coercivity since this multi-phase microstructure can switch the nucleation process of reverse domains into the domain wall pinning. This switching can be followed by observing the initial magnetization curve measured for MnBi alloy samples ball-milled for different times (see Fig. 8). As discussed below, during the ball-milling process the LTP MnBi decomposes into Bi and Mn and thus increases pinning centers, so the virgin magnetization curves switch from the behavior of coherent rotation to the pinning one leaving the kinks on this curves for the ball-milled samples. It is

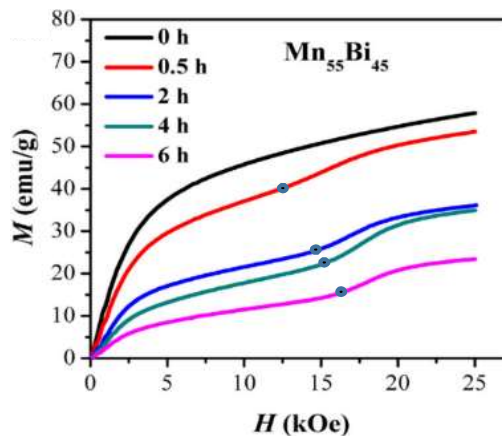


**Fig. 8.** The virgin  $M(H)$  curves of  $Mn_{55}Bi_{45}$  alloys ball-milled for 0 ÷ 6 h [20]. The black points remark the pinning fields.

worthy to note that the coercivity switching mechanism is dimed by the Bi accumulation, so the mentioned behavior of virgin magnetization curves is not standard for MnBi system and depends on the individual samples.

The temperature dependence of  $iH_c$  is specific for MnBi system, it is featured by the positive thermal coefficient  $d(iH_c)/dT > 0$ . This valuable specification extends the application of MnBi bulk magnets until  $\sim 473$  K, at which the  $(BH)_{\max}$  is kept on the level 6 MGOe [23] competitive with that of NdFeB magnets. The  $iH_c(T)$  is firstly discussed for MnBi ribbons samples in [8], where  $iH_c$  continuously increases by increasing  $T$  from 98 to 553 K (see Fig. 9a). The main reason supporting this useful dependence is the temperature dependent of the magnetocrystalline anisotropy energy coefficient  $K = K_1 + K_2$  as shown by the inset of Fig. 9a. This temperature dependence is conservative for other samples as bulk magnets prepared by the Spark Plasma Sintering at 533 K, 120 MPa for 30 s (sample SPS 1) and 120 s (SPS 2) and Hot Compaction at 200 MPa for 5 min. at 473 K (HC 1) and 573 K (HC 2) (see Fig. 9b).

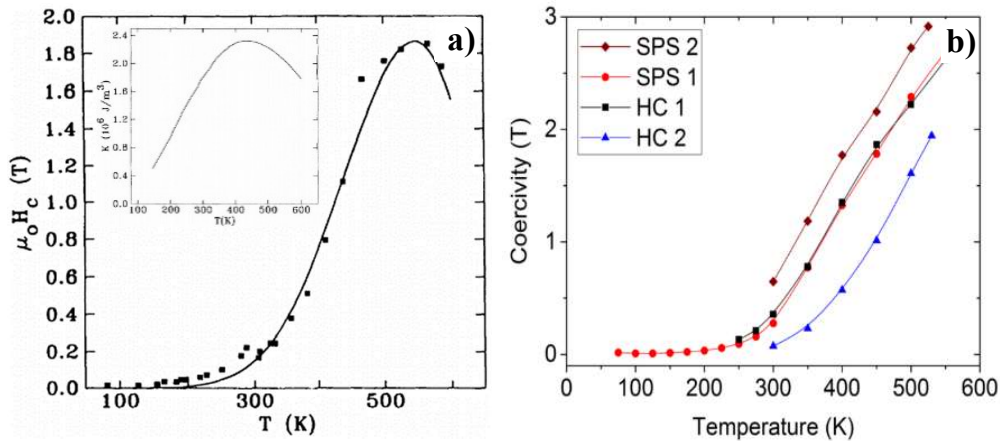


Fig. 9. The temperature dependent  $iH_c$  of MnBi ribbon (a) [8] and bulk magnets (b) [13].

### III. MnBi BULK MAGNETS

#### III.1. Bulk magnets

The goal of developing hard magnetic materials is closely related with their applications. Owing interesting application for magneto-optics [24] and thermo-magnetics [25], the application as high-temperature bulk magnets alternative to the high-cost NdFeB ones is expected as a great potential for low-cost MnBi magnets.

Despite numerous efforts spent, the past development of performance of MnBi bulk magnets is sluggish [26–38]. This history of development of  $(BH)_{\max}$  is summarized in Fig. 10. The starting value of 4.3 MGOe was obtained in 1952 year. The drop of  $(BH)_{\max}$  down to 2.3 MGOe was caused by using a binder (8 wt%) to compact powders into magnets. After 1960 year, the applications of MnBi based materials were focused for the magneto-optics and the storm development of rare-earth containing magnets annulled any attempts of MnBi bulk magnet development.

From 2010 year, where the world stood against the crisis of rare earth element prices, the study of MnBi magnets has been renewed. The numerous efforts of scientists created a fast growth of  $(BH)_{\max}$  during past 9 years and attend towards 12 MGOe for 2020 year.

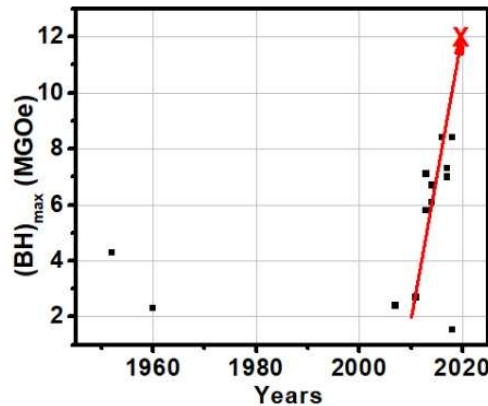


Fig. 10. The history of  $(BH)_{\max}$  values of prepared MnBi bulk magnets.

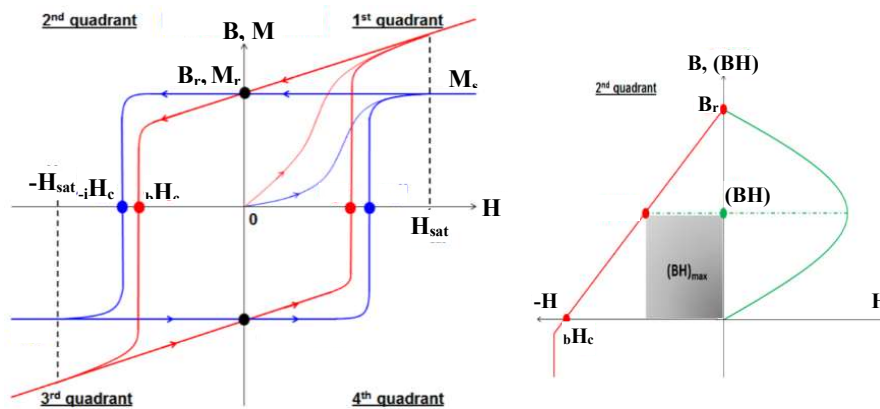


Fig. 11. The schematical  $M(H)$  and  $B(H)$  loops of an ideal magnet (left picture) and 2nd quadrant of  $B(H)$  loop of a MnBi magnet (right picture).

To discuss what is the near future of development of MnBi bulk magnets, one plots in Fig. 11 the  $M(H)$  and  $B(H)$  full quadrant loops of an ideal magnet. This type of loops can be observed, for example, for high-performance NdFeB dense magnets [39]. MnBi belongs to the type of materials of high magnetocrystalline anisotropy energy, so 2<sup>nd</sup> quadrant  $B(H)$  curve is linear and  $(BH)_{\max}$  can reach  $(bH_c \cdot B_r)/4$  if  $bH_c \geq B_r$ . Therefore, in order to maximize  $(BH)_{\max}$  one has maximize  $B_r$  (or  $M_r$ ) and  $bH_c$ .

To maximize  $M_r$ , one has to own high  $M_s$  and large ratio  $M_r/M_s$ . The value of  $M_s$  depends on the LTP content, the alignment degree of green powders and the sintering conditions. To

maximize  $bH_c$ , the magnet coercivity  $iH_c$  and the squareness  $\gamma$  must be kept high. The problems concerning the coercivity  $iH_c$  of magnets were considered above. The value of  $\gamma$  depends on the alignment degree, the value of  $iH_c$  and coercivity mechanism functioned in magnets. The status of physics and techniques to solve these problems is discussed in the next section.

### III.2. Towards making high-performance bulk magnets

The theoretical value of  $(BH)_{max}$  of MnBi bulk magnets can be estimated by the above formula  $(BH)_{max} = (bH_c \cdot Br)/4$  with the balance between  $bH_c$  in kOe and  $B_r$  in kG. By using  $M_s$  in the range of  $74 \div 81.3$  emu/g and  $\rho$  in the range  $8.6 \div 9.042$  g/cm<sup>3</sup>, the averaged value of the upper limit  $(BH)_{max}$  is 18.5 MGOe. The current value of  $(BH)_{max}$  is 8.4 MGOe [1] and is taken under a great focus for finding novel approaches to increase towards the upper limit value. It is worthy to note that the efforts spent in past time for searching novel approaches seem inefficient since the difficulties one faced with are fastened with the fundamental problems of MnBi system which will be considered below.

#### III.2.1. MnBi alloy LTP content improvement

Because of the peritectic nature of solidification, independent on the alloying methods used, the LTP content of Mn-Bi alloys is less than 30 wt%. The LTP content improvement, therefore, is necessary and up to now is made by using the isothermal annealing process. Since the annealing temperature  $T_a$  is restricted below 613 K, the annealing duration must be extended for a long time, from several tens of hours to several weeks. The mechanism of LTP enhancement during the isothermal annealing has been proved to be diffusive [40]. Because of the accumulation effect of Bi announced above, with the time the diffusion coefficient is decreased and annulled, so the full content 100 wt% of LTP should never reached.

To produce high LTP content MnBi alloys in massive scale, some non-traditional methods are tested, such as the temperature gradient assisted zonetravelling for LTP  $\sim 85$  wt% and the multi-time annealing with LTP up to 96 wt% [41]. The kilograms scale production has been also claimed in [42], where the vacuum heat treatment, milling and sieving steps are performed iteratively to achieve a fraction of LTP-MnBi in the high-purity alloy product greater than 95 wt%.

#### III.2.2. MnBi powder LTP content improvement

The high LTP-content MnBi alloys are the starting materials utilized in making green MnBi powders. The high LTP content creates the high value of  $M_s$ . Ordinarily, the coercivity  $iH_c$  of MnBi alloys is less than 1 kOe, so the green MnBi powders must be manufactured by grinding alloys for a long time to get the grain size preferred in the range 0.25 to 1  $\mu$ m, in order to increase  $iH_c$  (in kOe) more than the starting value  $M_s$  (in kG).

There is a bad effect occurred during the milling process which is featured specially for MnBi material. This effect is the LTP decomposition into Mn and Bi that occurs under collision force of milling. This effect depreciates the grinding process, since the coercivity enhancement becomes worthless once the LTP content and thus  $M_s$  is depressed. The decomposition effect was observed in all investigation works done for MnBi systems, that means the effect is closely connected with the thermodynamics of systems rather than with technical problems. The effect firstly was discussed in [43] but was skipped for a long time and is emphasized in [44], where the effect was depressed partly by using the dopants of Cu, Al. This decomposition effect is the main culprit of preventing the performance of MnBi bulk magnets and needs to be deeply explored and

solved in the near future in order to keep constant or to improve LTP content of MnBi ground powders.

### III.2.3. Balances required for compacting and sintering MnBi bulk magnets

Once we have a high- $iH_c$  and large- $M_s$  green powders, the high-performance bulk magnets cannot be produced automatically. The high performance of MnBi bulk magnets requires to keep following conditions: i) A high alignment degree of the in-mold aligned particles; ii) To optimize the pressure value applied for compacting the aligned particles into a green magnet; iii) To optimize the hot compaction sintering conditions.

The high alignment degree is the first requirement one has to warrantee in order to get anisotropic magnets. The alignment degree  $\zeta$  depends on the mutual directions of pressure and alignment field as well the strength of a magnetic field existed in the gap of an electric magnet.  $\zeta$  can be estimated by using the ratio between the intensity peaks MnBi<sub>(002)</sub> and MnBi<sub>(101)</sub> appeared on the XRD pattern taken from the magnet surface with normal vector parallel to the alignment field (parallel surface) related to the theoretical value 0.102 of this ratio. The coefficient  $\zeta$  is 1 for non-aligned magnets and reaches infinity for ideal textured magnets.

For example, the XRD pattern of parallel surface of MnBi in-epoxy aligned magnet under 18 kOe field is presented in Fig. 12a. Because of the high alignment degree, the peaks (002) and (004) appear strongly and the rest of peaks is disappeared. The coefficient  $\zeta$  of this in-epoxy bonded magnet is 258.

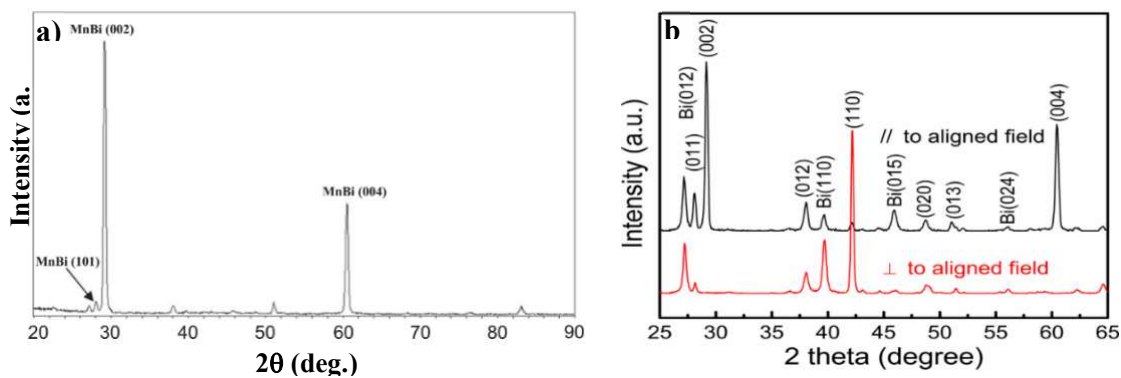


**Fig. 12.** (a) The XRD pattern of parallel surface of in-epoxy highly aligned MnBi particles [33], (b) The XRD pattern of parallel and perpendicular surfaces of a MnBi bulk magnet [34].

In practice, because the bulk magnet is aligned in a mold, so the rotation of particles is not free, so the coefficient  $\zeta$  of real bulk magnets is less than that of the in-epoxy bonded magnet. Fig. 12b plots the typical XRD pattern of in-mold aligned, compacted and sintered MnBi bulk magnet. In comparison with Fig. 12a, the XRD patterns of parallel and perpendicular surfaces of the magnet contain all peaks of MnBi phase. However, the texture of peaks of these two surfaces is different. On the XRD pattern of perpendicular surface the peak (002) disappears, the ratio  $I_{MnBi(002)}/I_{MnBi(101)}$  is zero. In contrary, on the XRD pattern of parallel surface the peak (002) is enhanced, the ratio  $I_{MnBi(002)}/I_{MnBi(101)} = 4.8$ , thus the alignment degree of this magnet  $\zeta$  is 47.4.

After aligning in a field, the assembly of aligned and magnetized particles must be compacted into a green compact used for sintering magnets. By applying a compact pressure  $P$ , the distances between particles decrease, the mass density of the green compact increases. However, this increase of density should affect the magnetostatic field of the compacted system and can decrease the coercivity  $iH_c$  of the green compact in order to minimize the energy of the compact system. These both contrary processes lead to an optimal value of  $P_{opt}$  which creates a good balance between the mass density and  $iH_c$  of magnets. The practical value of  $P_{opt}$  depends on the mold construction and was announced, for example, equal 1800 – 2000 psi in Refs. [23, 33, 34].

It is clear that, the sintering conditions affect directly the magnetic properties of final magnet products. For MnBi system, the following attentions must be paid: i) the sintering temperature  $T_{ma}$  must be lower than 613 K and higher 544°C. The first value corresponds to the upper limit, over which the LTP can be destroyed. The second value is the melting temperature of Bi, over which the sintering process occurs intensively; ii) the sintering time  $t_{ma}$  must be short, around some tens minutes to avoid any destroys of LTP content; iii) the sintering must be conducted under pressure  $P_{ma}$ , by other word the hot compaction procedure must be dealt with. The practical values are  $T_{ma} \sim 573$  K,  $t_{ma} \sim 10 - 30$  min.,  $P_{ma} \sim 2000$  psi [23, 33, 34].

The current best MnBi bulk magnet was prepared almost by using the above mentioned procedures. The  $(BH)_{max}$  is 8.4 MGOe, The  $M(H)$  loops are shown in Fig. 13 [34].

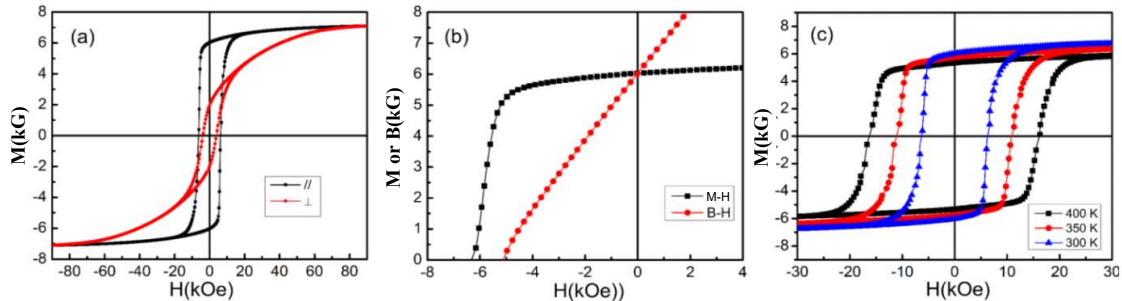


**Fig. 13.** (a)  $M(H)$  loops of MnBi magnet measured at 9 Tesla field parallel ( $//$ ) and perpendicular ( $\perp$ ) fields, (b)  $M$ ,  $B(H)$  curves of the magnet measured at RT parallel field and (c)  $M(H)$  of the magnet measured at 300, 350 and 400K parallel to alignment field direction [34].

#### IV. CONCLUSIONS

The paper gives a critical review on the magnetism of rare-earth-free hard magnetic MnBi material. The crystal structure, the phase microstructure and the related spontaneous magnetization and coercivity are presented and discussed in detail. The actual problems to be solved in order to enhance further the performance of MnBi bulk magnets are discussed critically.

The paper emphasizes, that the destiny of further development of MnBi magnets is closely connected with the ferromagnetic phase (LTP) decomposition effect which occurs intensively under impact forces. This effect prevents any efforts to produce high-performance MnBi green powders used for making high-performance MnBi bulk magnets. This effect is fundamental, the

mechanism of which is not clear and the numerous approaches tested until today are not sufficient to depress or cancel it. So, the first priority must be seriously paid for studying and solving this effect. Once this decomposition is restricted or cancelled, low-cost bulk magnets with  $(BH)_{max} \sim 10\text{--}12$  MGOe at RT and  $6\text{--}8$  MGOe at  $423\text{--}473$  K ( $150\text{--}200^\circ\text{C}$ ) will be produced in a large scale and will join the world magnet market.

## ACKNOWLEDGMENTS

This research is funded by Vietnam National Foundation for Science and Technology Development (NAFOSTED) under Grant Number 103.02-2017.327.

## REFERENCES

- [1] J. Cui, J. P. Choi, G. Li, E. Polikarpov, J. Darsell, N. Overman, M. Olszta, D. Schreiber, M. Bowden, T. Droubay, M. J. Kramer, N. A. Zarkevich, L. L. Wang, D. D. Johnson, M. Marinescu, I. Takeuchi, Q. Z. Huang, H. Wu., H. Reeve, N. V. Vuong and J. P. Liu, *J. Phys.: Condens. Matter* **26** (2014) 064212.
- [2] Michael E. McHenry, Matthew A. Willard, David E. Laughlin, *Progress in Materials Science* **44** (1999) 291.
- [3] V. Seshu Bai and T. Rajasekharan, *J. Magn. Magn. Mater.* **42** (1984) 198.
- [4] H. Gobel, E. Wolfgang, and R. Harm, *Phys. Stat. Sol. (a)* **34** (1976) 553.
- [5] T. J. Williams, A. E. Taylor, A. D. Christianson, S. E. Hahn, R. S. Fishman, D. S. Parker, M. A. McGuire, B. C. Sales, and M. D. Lumsden, *Appl. Phys. Lett.* **108** (2016) 192403.
- [6] V. V. Nguyen, C. Rong, Y. Ding, and J. Ping Liu, *J. Appl. Phys.* **111** (2012) 07A731.
- [7] Y. B. Yang, X. G. Chen, S. Guo, A. R. Yan, Q. Z. Huang, M. M. Wu, D. F. Chen, Y. C. Yang, J. B. Yang, *J. Magn. Magn. Mater* **330** (2013) 106.
- [8] X. Guo, X. Chen, Z. Altounian, and J. O. Strom-Olsen, *Phys. Rev. B* **46** (1992) 14578.
- [9] J. Park, Y. K. Hong, J. Lee, W. Lee, S. G. Kim and C. J. Choi, *Metals* **4** (2014) 455.
- [10] R. R. Heikes, *Phys. Rev.* **99** (1955) 446.
- [11] B. D. Cullity, C. D. Graham, *Introduction to Magnetic Materials*, John Wiley & Sons, (2005), ISBN 0-201-01218-9.
- [12] H. Kronmuller and M. Fahnle, *Micromagnetism and Microstructure of Ferromagnetic Solids* (2003), Cambridge University Press, Cambridge.
- [13] S. Muralidhar, J. Grafe, Y. C. Chen, M. Etter, G. Gregori, S. Ener, S. Sawatzki, K. Hono, O. Gutfleisch, H. Kronmuller, G. Schutz, and E. J. Goering, *Phys. Rev. B* **95** (2017) 024413.
- [14] R. G. Pirich and D. J. Larson, Jr. Grumman Aerospace Corporation, Betpahe, N. Y. , *Patent # USA4784703*, Nov. 15, 1988.
- [15] J. Fischbacher, A. Kovacs, H. Oezelt, M. Gusenbauer, T. Schrefl, L. Exl, D. Givord, N. M. Dempsey, G. Zimanyi, M. Winklhofer, G. Hrkac, R. Chantrell, N. Sakuma, M. Yano, A. Kato, T. Shoji, and A. Manabe, *Appl. Lett.* **111** (2017) 072404.
- [16] M. Kishimoto and K. Wakai, *Jap. J. Appl. Phys.* **15** (1976) 549.
- [17] M. Kishimoto and K. Wakai, *Jap. J. Applied Phys.* **16** (1977) 459.
- [18] R. Liu, M. Zhang, E. Niu, Z. Li, X. Zheng, R. Wu, W. Zuo, B. Shen, F. Hu, and J. Sun. *J. Appl. Phys.* **115** (2014), 17A742.
- [19] Z. Xiang, Y. Song, D. Pan, Y. Shen, L. Qian, Z. Luo, Y. Liu, H. Yang, H. Yan, W. Lu, *J. All. Comp.* **744** (2018) 432.
- [20] J. Cao, Y.L. Huang, Y.H. Hou, Z.Q. Shi, X.T. Yan, Z.C. Zhong, G.P. Wang, *J. Magn. Magn. Mater.* **473** (2019) 505.
- [21] K. Oikawa, Y. Mitsui, K. Koyama and K. Anzai, *Materials Transactions* **52** (2011) 2032.2039.
- [22] V. V. Nguyen, T. X. Nguyen. *J. Elec. Mater.* **46** (2017) 3333.
- [23] V. V. Nguyen, N. Poudyall, X. B. Liu, J. Ping Liu, K. Sun, M. J. Kramer and J. Cui, *Mater. Res. Exp.* **1** (2014) 036108.
- [24] R. F. Sabiryanov and S. S. Jaswal, *J. Appl. Phys.* **85** (1999) 5109.

- [25] C. Curcio, E. S. Olivetti, L. Martino, M. Küpferling and V. Basso, *Solid State Phenomena* **257** (2016) 143.
- [26] E. Adams, W. M. Hubbard, and A. M. Syeles, *J. Appl. Phys.* **23** (1952) 1207.
- [27] N. Makino and M. Suzuki, *J. of the Japan Institute of Metals* **24** (1960) 24.
- [28] K.Y. Ko, S.J. Choi, S.K. Yoon and Y.S. Kwon, *J. Magn. Magn. Mater.* **310** (2007) e887.
- [29] D. T. Zhang, S. Cao, M. Yue, W. Q. Liu, J. X. Zhang and Y. Qiang, *J. Appl. Phys.* **109**, (2011) 07A722.
- [30] N. V. Rama Rao, A. M. Gabay and G. C. Hadjipanayis, *J. Phys. D: Appl. Phys.* **46** (2013) 062001.
- [31] N. V. Rama Rao, A. M. Gabay, and G. C. Hadjipanayis, *IEEE Trans. Magn.* **49** (2013) 3255.
- [32] K. W. Moon, K. W. Jeon, M. Kang, M. K. Kang, Y. Buyn, J. B. Kim, H. Kim, and J. Kim, *IEEE Trans. Magn.* **50** (2014) 2103804.
- [33] V. V. Nguyen, N. Pouydal, X. Liu, J. Ping Liu, K. Sun, M. J. Kramer, and J. Cui. *IEEE Trans. Magn.* **50** (2014) 2105506.
- [34] N. Poudyal, X. Liu, W. Wang, V. V. Nguyen, Y. Ma, K. Gandha, K. Elkins, J. Ping Liu, K. Sun, M. J. Kramer, and J. Cui, *AIP Advances* **6** (2016) 056004 .
- [35] S. Kim, H. Moon, H. Jung, S. M. Kim, H. S. Lee, H. Choi-Yim, W. Lee. *J. All. Comp.* **708** (2017) 1245.
- [36] V. V. Nguyen, T. X. Nguyen, *Alloys and Magnets. J. Elec. Mater.* **46** (2017) 3333.
- [37] V. V. Nguyen, T. X. Nguyen, *Physica B* **532** (2018) 103.
- [38] J. Cao, Y. L. Huang, Y. H. Hou, G. Q. Zhang, Z. Q. Shi, Z. C. Zhong, and Z. W. Liu, *AIP Advances* **8** (2018) 055132.
- [39] J. Chen , D. Wang, S. Cheng, Y. Jiang, X. Teng, Z. Chen, Y. Shen, F. Birkammer, and D. Gerling, *IEEE Trans. Magn.* **54** (2017) 1.
- [40] V. V. Nguyen Van Vuong, T. X. Nguyen, *J. Sci. Tech.* **54** (1A) (2016) 50.
- [41] T. X. Nguyen, V. V. Nguyen, *J. Mater. Sci.: Mater. in Electronics.* March (2019), <https://doi.org/10.1007/s10854-019-01003-x>.
- [42] J. P. Choi, C. A. Lavender, G. Li and J. Cui. Battelle Memorial Institute, Richland, WA (US). Patent US 2015/0110664 A1, Apr. 23, 2015.
- [43] F. Yin, N. Gu, T. Shigematzu, N. Nakanishi. *J. Mater. Sci. Technol.* **12** (1996) 335.
- [44] V.V. Ramakrishna, S. Kavita, Ravi Gautam, T. Ramesh, R. Gopalan, *J. Magn. Magn. Mater.* **458** (2018) 23.